Journal of Molecular Liquids 253 (2018) 72–82

Contents lists available at ScienceDirect

Journal of Molecular Liquids

journal homepage: www.elsevier.com/locate/molliq

Synthesis of zeolite nanostructures from waste aluminum cans for efficient removal of malachite green dye from aqueous media

Ehab A. Abdelrahman

Chemistry Department, Faculty of Science, Benha University, Benha 13518, Egypt

ARTICLE INFO

Article history:
Received 8 November 2017
Received in revised form 20 December 2017
Accepted 7 January 2018
Available online 08 January 2018

Keywords:
Zeolite nanostructures
Wastes
Aluminum cans
Malachite green dye
Water treatment

ABSTRACT

Different zeolite nanostructures were synthesized from waste aluminum cans via a low-cost hydrothermal method using different silicon sources. The produced nanostructures were identified using XRD, FT-IR, SEM, and TEM analyses. XRD proved that the samples which synthesized using fumed silica and sodium metasilicate consist of a composite of (analcime, hydroxysodalite, and zeolite P1) and (sodium aluminum silicate hydroxide hydrate and nepheline hydrate), respectively. Moreover, the samples which synthesized using silica gel and tetraethyl orthosilicate composed of LTA zeolite and a composite of (sodium aluminum silicate hydroxide hydrate and zeolite 4A), respectively. The as-prepared zeolite nanostructures were tested in the removal of malachite green dye from aqueous media using a batch method. The results revealed that the adsorption processes fitted well with the pseudo-second-order kinetic model and Langmuir adsorption isotherm. In addition, the mechanism of adsorption processes was controlled by three successive stages, namely inner diffusion, outer diffusion, and pore diffusion processes where the pore diffusion is the rate-determining step. Additionally, thermodynamic parameters showed that the adsorption processes were spontaneous, physisorption, and exothermic.

1. Introduction

Rubbish is a mixture of stones, dust, sand, wood, metal, leather, and various wastes (such as paper, porcelain, and glass). This is the widespread expression of so-called waste or solid waste, which is produced by human activities from various walks of life (housing, camp, service facilities, etc.). The accumulation of rubbish without disposal causes a lot of health problems that become a fertile breeding ground for microbes, animals, and insects such as flies, mosquitoes, mice, cats, and dogs. This helps spread diseases that affect human health [1]. It also affects the tourist activity and damages the basic buildings of roads, waterways, and sewage. The psychological and social effects of the citizens were also increased because of the accumulation of rubbish and fearing of the spread of diseases among them. In developed countries, rubbish is used in the development of some industries. This helps significantly in reducing the quantities of rubbish that will be disposed of in landfills. Also, the benefits that will accrue to the national economy from the use and recycling of such wastes were increased.

Waste from homes is not scarce. Rubbish collected in the United States is estimated to be equivalent to half a kilogram of household waste per person per day. Also, it is well known that the problem of rubbish is one of the major problems that most of the inhabitants of the villages and regions of Egypt suffer from. It is one of the most important problems that must be taken care of and work to solve. This is because of the excellent environmental and financial returns in the case of economic exploitation instead of leaving it to accumulate. Most of these wastes can be utilized after separating the components of it into different types, which include: paper [2, 3], glass [4–7], plastic [8–10], agricultural [11, 12], and metallic wastes [13–16]. Metallic wastes, such as aluminum wastes, are very important as it is converted into factories for melting and recycling them again. This process involves only metal smelting, which is less expensive and energy consuming than the preparation of new aluminum by electrolysis of aluminum oxide. This is due to the electrolysis process need to extract bauxite ore [17, 18]. Aluminum cans such as 7 up cans are a wealth of themselves. It is one of the best waste recycling projects because aluminum is the economic packing material in its assembly and recycling. Scientists have recently sought to exploit some aluminum wastes in the preparation of aluminum oxide [19, 20] and hydrotalcite [21] nanomaterials. Also, silicon wastes were used in the preparation of nanomaterials called zeolites with

E-mail addresses: dr.ehabsaleh@yahoo.com, ehab.abdelrahman@fsc.bu.edu.eg,
URL: http://www.bu.edu.eg/staff/ehababdelrahman7.

https://doi.org/10.1016/j.molliq.2018.01.038
0167-7322/

great industrial applications [22–26]. Zeolites are a highly porous material made up of crystals of aluminum silicates [27]. These substances are able to retain positive ions such as the Na^+, K^+, Ca^{2+}, and Mg^{2+} in their pores. These materials have many characteristics that make them have environmental, industrial, agricultural and economic applications [28–40]. Removal of organic dyes from aqueous solutions is one of the most important benefits of zeolites, as these dyes are dangerous to human health [41–47]. There are different ways to prepare such zeolites compounds using the hydrothermal method [48–59]. But these methods depend on the use of high-cost chemicals for aluminum sources. As far as I know, there are no papers yet in the preparation of zeolite from the cans. So this was motivating me to work at that point. In this research paper, 7 up aluminum cans were used as a cheap aluminum source which available in the rubbish. Different zeolite nanostructures were synthesized using the hydrothermal method. This can be achieved through the interaction between the aluminum source solution and a solution of different sources of silica namely fumed silica, sodium metasilicate, silica gel, and tetraethyl orthosilicate. Also, the synthesized zeolite nanostructures were used to purify water from the malachite green dye.

2. Experimental

2.1. Chemicals

The chemicals used in this paper are sodium hydroxide (NaOH), silica gel (SiO_2), fumed silica (SiO_2), sodium metasilicate ($Na_2SiO_3 \cdot 5H_2O$), tetraethyl orthosilicate ($Si(OC_2H_5)_4$), and malachite green dye ($C_{23}H_{25}ClN_2$). All of which was purchased from Sigma-Aldrich company. 7 up cans (which containing aluminum) were collected from the local Egyptian market.

2.2. Synthesis of zeolite nanostructures

The aluminum solution has been prepared as follows: 2 g of the outer part of the 7 up cans was dissolved in 50 ml of 2.5 M sodium hydroxide solution. Then the resulting solution was filtered to remove impurities. While the silicon solution was prepared by dissolving 2.25 g of silicon from different silicon sources in 50 ml of 2.5 M sodium hydroxide solution. The silicon sources used were fumed silica (4.80 g), sodium metasilicate (17.07 g), silica gel (4.80 g), and tetraethyl orthosilicate (16.76 g). After that, the previous two solutions were added to each other partially wise with continuous stirring for 30 min. Then, the produced gel was transferred to the Teflon lined stainless autoclave. For the hydrothermal treatment, the autoclave was placed at 150 °C for one day. Afterward, the precipitates were filtered, washed thoroughly several times with bidistilled water, and dried at 120 °C for 12 h. It noteworthy that the samples synthesized using fumed silica, sodium metasilicate, silica gel, and tetraethyl orthosilicate were labeled as ZF, ZM, ZS, and ZT, respectively.

2.3. Adsorption study

Using 100 ml beakers, 0.1 g of the sample prepared using fumed silica (ZF) or sodium metasilicate (ZM) was added to 50 ml of the malachite green dye solution (700 mg/l). The above steps were repeated with the samples prepared using silica gel (ZS) or tetraethyl orthosilicate (ZT) but with 50 mg/L malachite green dye solution. After that, the solutions were stirred at room temperature using a multi-position magnetic stirrer (550 rpm). After the arrival of the time required for the adsorption study, the contents of beakers were separated using the centrifuge (3000 rpm). The residual concentration of the dye (after adsorption process) was measured using the UV -Vis spectrophotometer at 620 nm (λ_{max} of malachite green dye) utilizing their pre-constructed calibration curves. The adsorption capacity of the adsorbent materials at time t (Q_t, mg/g) was measured using Eq. (1).

$$Q_t = (C_o - C_t)V/m \quad (1)$$

where, C_o (mg/l) is the initial concentration of malachite green dye solution, C_t is the residual concentration of malachite green dye at time t, V (l) is the volume taken of the malachite green dye solution, and m (g) is the mass of adsorbent materials. It is noteworthy that the percent removal of malachite green dye (% Removal) at time t was estimated using Eq. (2)

$$\%\text{Removal} = (C_o - C_t)100/C_o \quad (2)$$

Moreover, the effect of different concentrations of malachite green dye (200-1000 mg/l, in case of ZF or ZM and 10-200 mg/l, in case of ZS or ZT) has been studied. The adsorption capacity of the adsorbent materials at equilibrium (Q_e, mg/g) was measured using Eq. (3).

$$Q_e = (C_o - C_e)V/m \quad (3)$$

where, C_e (mg/l) is the concentration of malachite green dye solution at equilibrium.

In addition, the percent removal of malachite green dye (% Removal) at equilibrium was calculated using Eq. (4)

$$\%\text{Removal} = (C_o - C_e)100/C_o \quad (4)$$

Also, the effect of three temperatures (298, 313 and 323 K) on the malachite green dye solution of concentration 700 mg/l (in the case of ZF or ZM) or 50 mg/l (in the case of ZS or ZT) has been studied. The adsorption capacity of the adsorbent materials at different temperatures (Q_T, mg/g) was measured using Eq. (5).

$$Q_T = (C_o - C_T)V/m \quad (5)$$

where, C_T is the residual concentration of malachite green dye at temperature T. In addition, the percent removal of malachite green dye (% Removal) at temperature T was calculated using Eq. (6)

$$\%\text{Removal} = (C_o - C_T)100/C_o \quad (6)$$

2.4. Physico-chemical measurements

XRD patterns of the as-prepared zeolite nanostructures samples (ZF, ZM, ZS, and ZT) were detected using an 18 kW diffractometer (Bruker; model D8 Advance) equipped with monochromated Cu Kα radiation ($\lambda = 1.54178$ Å). FT-IR spectra of the as-prepared zeolite nanostructures samples were collected using a Nicolet iSio FT-IR spectrophotometer in the 4000-400 cm^{-1} region using KBr disk. The SEM images of the as-prepared zeolite nanostructures samples were taken on a scanning electron microscope (JEOL; model JSM-6510LA). Elemental analyses of 7 up cans and the as-prepared zeolite nanostructures samples were performed using link, ISIS-300, Oxford EDS (energy dispersion spectroscopy) detector. The TEM images of zeolite nanostructures samples on carbon-coated grids (CCG) were collected employing a transmission electron microscope (JEOL-1010) at a speeding voltage of 80 kV.

3. Results and discussion

3.1. XRD and EDS studies

The EDS analysis of the outer shell of the 7 up cans proved that it contains C, O, Mg, Al, Si, Ti, Mn, and Fe as shown in Fig. 1 and Table 1. It is also clear that aluminum occupies the highest ratio (31.22%). X-

ray diffraction (XRD) technique is a family of analytical techniques that gives information about the crystalline structure and chemical composition. It is proved that the sample which prepared using fumed silica (ZF) consists of composites of different phases of zeolite includes analcime (Cubic; JCPDS No. 70-1575; Space group: Ia-3d) [60], hydroxysodalite (Cubic; JCPDS NO. 11-0401; Space group: P-43n) [61], and zeolite P1 (Tetragonal, JCPDS No. 39-0219; Space group: I-4) [62] as strongly shown in Fig. 2A and Table 2. It is also worth mentioning that the results of X-ray diffraction proved that the sample which synthesized using sodium metasilicate (ZM) consists of composites of sodium aluminum silicate hydroxide hydrate (Cubic; JCPDS NO. 42-0215; Space group: P-43n) [63] and nepheline hydrate as shown in Fig. 2B and Table 2. It is known that the crystal system of nepheline hydrate is not yet known [64, 65]. In addition, XRD proved that the sample which synthesized using silica gel (ZS) composed of LTA zeolite (Cubic, JCPDS No. 73-2340; Space group: Fm-3c) as shown in Fig. 2C and Table 2 [66]. Moreover, The XRD confirmed that the sample which synthesized using tetraethyl orthosilicate (ZT) consists of composites of sodium aluminum silicate hydroxide hydrate (Cubic; JCPDS NO. 42-0215; Space group: P-43n) [63] and zeolite 4A (Cubic; JCPDS NO. 43-0142; Space group: Fm-3c) as shown in Fig. 2D and Table 2 [67]. Scherrer equation is an equation used to calculate the crystallite size (D, nm) of the nanoparticles and is given by the relationship in Eq. (7):

$$D = 0.9\lambda/\beta \cos\theta_B \quad (7)$$

where, β, θ_B, and λ are the full width at half maximum (FWHM) of the XRD diffraction peaks, the diffraction angle according to Bragg formula, and wavelength of the X-ray radiation, respectively [68–70]. It was found that the average crystallite size was increased according to the following order; ZM < ZT < ZF < ZS as clarified in Table 2. It is noteworthy that EDS analysis has shown that all synthesized samples (ZF, ZM, ZS, and ZT) are composed of high percent's of Na, O, Si and Al, as well as small percent's of Mg, Ti, Mn, and Fe as clarified in Table 1. It is also noted that Si/Al ratio of the aforementioned samples are 1.46, 126, 1.32, and 1.12, respectively. It is worth mentioning that XRD not detects any phases due to Mn, Mg, Fe, and Ti elements despite EDS confirm these elements. This is due to the small percents of those elements in the synthesized samples [70].

3.2. SEM and TEM studies

Morphologies of the as-prepared zeolite nanostructures products (ZF, ZM, ZS, and ZT) have been examined using both of scanning electron microscopy (SEM) and transmission electron microscopy (TEM), as shown in Figs. 3 and 4, respectively. The images taken by SEM demonstrated that ZM and ZT samples are made up of aggregates of a sphere like structures with an average size of ca.3.54 and 3.07 μm, respectively. In addition, ZF and ZS samples were found to consist of aggregates of a (sphere and sheet) and (sphere and cubic) like structures with an average size of ca. 10.33 and 8.65 μm, respectively. Moreover, TEM images, exhibit that the samples; ZF, ZM, ZS, and ZT, are composed of spherical, (spherical and irregular), (spherical and cubic), and spherical shape particles with average diameters of 46.56, 26.28, 75.83, and 38.73 nm, respectively. These results are in agreement with those deduced from XRD analysis. The above results can be explained by the fact that the change of the silicon source results in an effect on the produced phase, crystallite size, and morphology [51, 71].

Table 1
EDS data of the 7 up cans and the synthesized ZF, ZM, ZS, and ZT samples.

Sample	C%	Na%	O%	Mg%	Al%	Si%	Ti%	Mn%	Fe%
7 up cans	45.73	–	13.77	1.33	31.22	1.76	4.83	0.91	0.45
ZF	–	15.42	37.71	1.50	17.76	25.95	0.75	0.43	0.48
ZM	–	21.24	37.45	1.68	16.69	20.96	1.31	0.35	0.32
ZS	–	14.93	37.82	1.15	18.97	25.11	1.43	0.41	0.18
ZT	–	16.34	36.11	2.44	20.02	22.38	0.51	1.55	0.65

3.3. FT-IR study

Fig. 5 (A, B, C, and D) represents FT-IR spectra of the as-prepared zeolite nanostructures products (ZF, ZM, ZS, and ZT), respectively. The results revealed that the peaks which appeared at 3424, 3514, 3447, and 3430 cm^{-1} for ZF, ZM, ZS, and ZT samples, respectively are due to stretching vibration of surface adsorbed zeolite water. Also, the peaks at 1636, 1649, 1654, and 1635 cm^{-1} for ZF, ZM, ZS, and ZT samples, respectively assigned to bending vibration of HOH. Asymmetric stretching vibration (External; internal) of T-O (T = Si, Al) for ZF, ZM, ZS, and ZT samples are (1462; 1029 cm^{-1}), (1480; 987 cm^{-1}), (1454; 996 cm^{-1}), and (1459; 993 cm^{-1}), respectively. Moreover, symmetric stretching vibration (External; internal) for T-O (T = Si, Al) for ZF, ZM, ZS, and ZT samples are (740; 618 cm^{-1}), (699; 632 cm^{-1}), (667 cm^{-1}; not appear), and (723; 663 cm^{-1}), respectively. It is noteworthy to mention that double ring vibration for ZM, ZS, and ZT samples were observed at 563, 557, and 560 cm^{-1}, respectively.

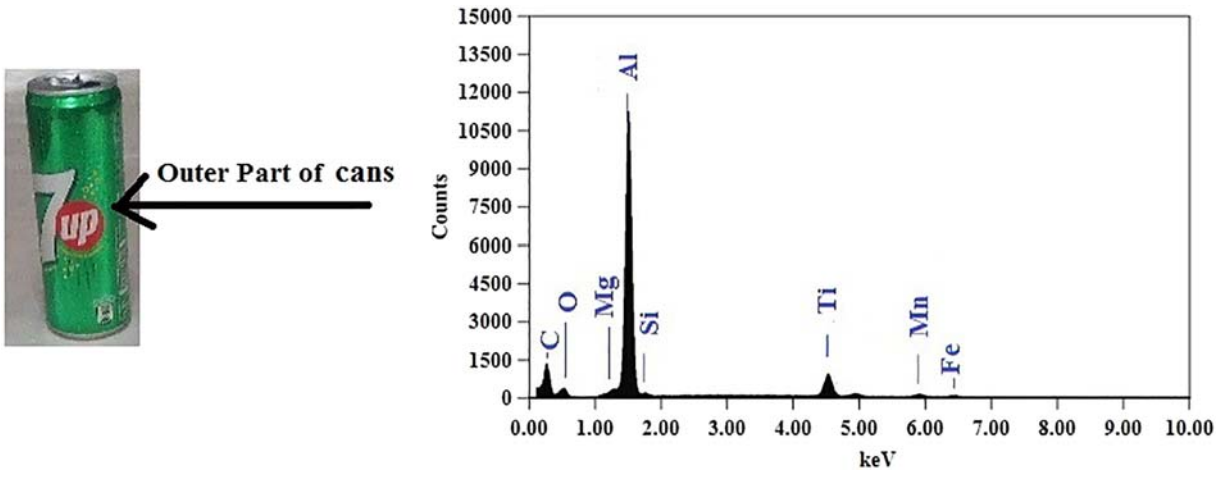

Fig. 1. The EDS spectrum of the outer part of 7 up cans.

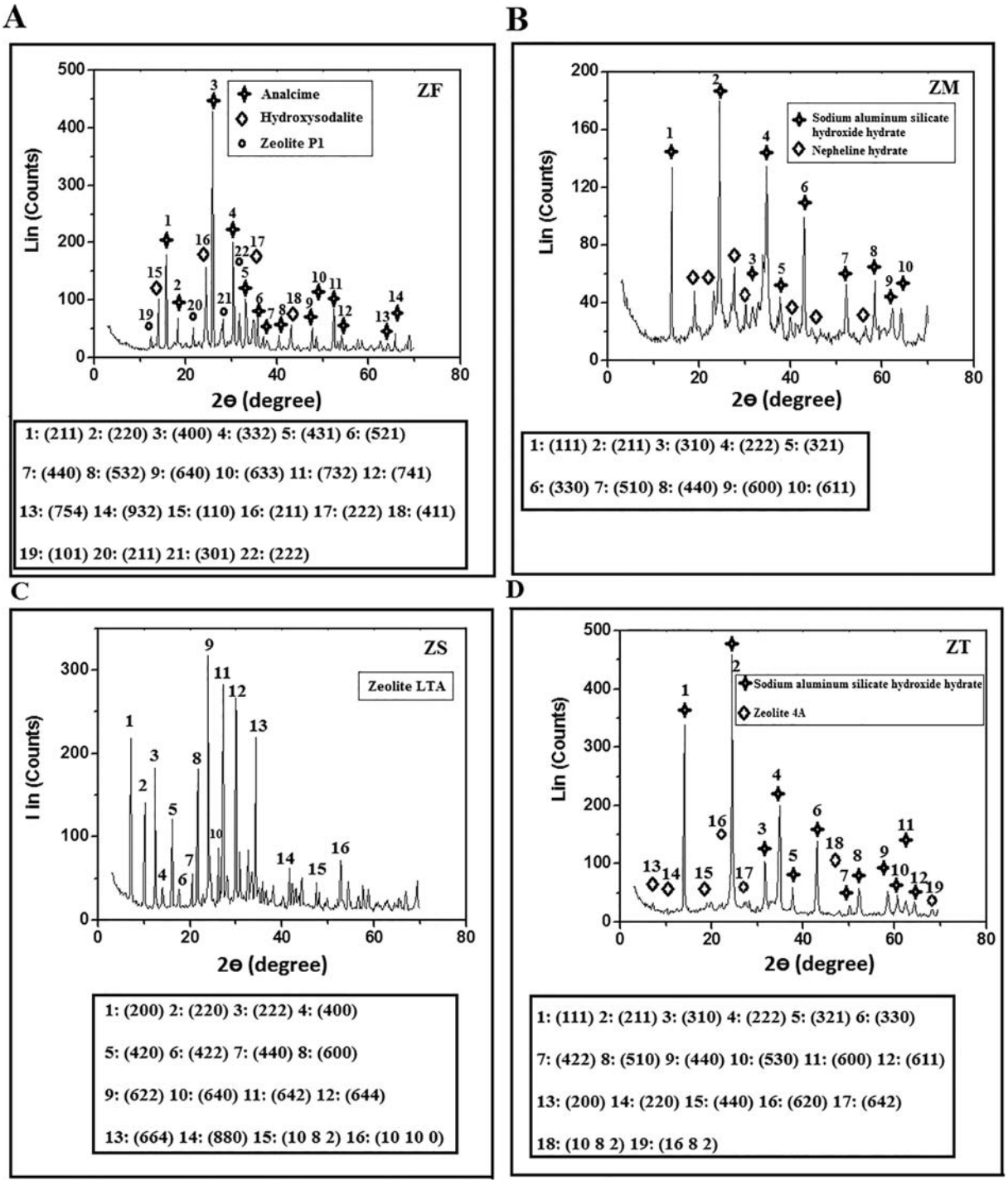

Fig. 2. XRD patterns of the zeolite nanostructures synthesized using fumed silica (ZF sample) (A), sodium metasilicate (ZM sample) (B), silica gel (ZS sample) (C), and tetraethyl orthosilicate (ZT sample) (D).

Table 2
Produced phases, chemical structure, JCPDS card, and average crystal size of the synthesized ZF, ZM, ZS, and ZT samples.

Sample	Produced phases	Chemical structure	JCPDS card	Average crystal size (nm)
ZF	Analcime	$Na\ (AlSi_2O_6)\ (H_2O)$	70-1575	57.77
	Hydroxysodalite	$Na_4Al_3Si_3O_{12}\ (OH)$	11-0401	
	Zeolite P1	$Na_6Al_6Si_{10}\ O_{32}\cdot 12H_2O$	39-0219	
ZM	Sodium aluminum silicate hydroxide hydrate	$Na_8\ (AlSiO_4)_6\ (OH)_2\cdot 2H_2O$	42-0215	21.89
	Nepheline hydrate	$Na_2Al_2Si_2O_8\cdot 0.5H_2O$	10-0459	
ZS	Zeolite LTA	$Na_{12}Al_{12}Si_{12}O_{48}\ (H_2O)_{27}$	73-2340	73.46
ZT	Sodium aluminum silicate hydroxide hydrate	$Na_8\ (AlSiO_4)_6(OH)_2\cdot 2H_2O$	42-0215	44.17
	Zeolite 4A	$Na_{92}Al_{92}Si_{100}\ O_{384}$	43-0142	

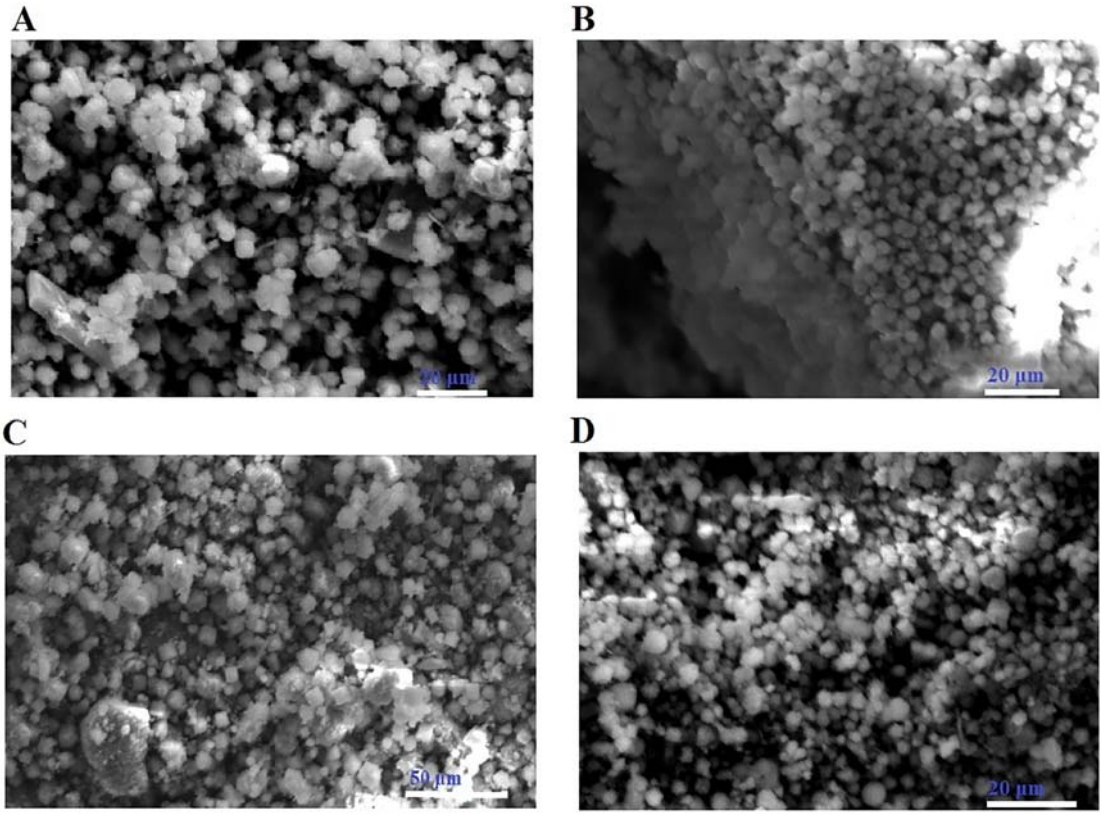

Fig. 3. SEM images of the zeolite nanostructures synthesized using fumed silica (ZF sample) (A), sodium metasilicate (ZM sample) (B), silica gel (ZS sample) (C), and tetraethyl orthosilicate (ZT sample) (D).

3.4. Adsorption of malachite green dye from polluted water using the as-prepared zeolite nanostructures

3.4.1. Effect of contact time and adsorption kinetics

Fig. 6 shows the relationship between the percent removal (Fig. 6A) or the amount of adsorbed dye (Fig. 6B) and the contact time. ZF, ZM, ZS, and ZT were found to have the highest percent removal of ca. 67.86, 78.57, 87.56, and 85.62 at equilibrium times of 120, 180, 40 and 50 min, respectively. Also, amounts of adsorbed dye were ca. 237.50, 275.00, 21.89, and 21.41 mg/g at the previous equilibrium times, respectively. Moreover, above equilibrium times the percent removal or the amount of adsorbed dye is not significantly affected because of the saturation of the active sites of the adsorbents. Six kinetic models were studied, to determine the mechanism of adsorption, [47] include Pseudo-first-order (Eq. (8)), Pseudo-second-order (Eq. (9)), Intra-particle-diffusion (Eq. (10)), Spahn and Schlunder (Eq. (11)), Iqbal et al. (Eq. (12)), and Bangham (Eq. (13)).

$$\log(Q_e - Q_t) = \log Q_e - K_1\, t/2.303 \tag{8}$$

$$t/Q_t = \left(1/K_2 Q_e^{\,2}\right) + (1/Q_e)\, t \tag{9}$$

$$Q_t = K_{int} t^{0.5} + C \tag{10}$$

$$\ln C_t = \ln C_o - K_{ext} t \tag{11}$$

$$\ln(1-F) = -K_{ext} t \tag{12}$$

$$\log R = \log[K_o m/2.303\, V] + \alpha \log t \tag{13}$$

where, Q_e (mg/g) is the amount of the adsorbed dye at equilibrium, Q_t (mg/g) is the amount of the adsorbed dye at time t (min), k_1 (1/min) is the pseudo- first-order rate constant, k_2 (g/mg.min) is the pseudo-second-order rate constant, C (mg/g) is the thickness of boundary layer, k_{int} (mg/(g.min$^{0.5}$)) is internal diffusion constant, K_{ext} (1/min) is external diffusion constant, C_t (mg/L) is the concentration of dye at time t, F is fraction attainment of equilibrium or extent of conversion and it was calculated using Eq. (14), α (mg/g.min) <1) and K_o (g/mg. min) are the Bangham constants. In addition, R can be calculated using Eq. (15)

$$F = Q_t/Q_e \tag{14}$$

$$R = \log[C_o/(C_o - Q_t m)] \tag{15}$$

Fig. 7 (A-F) represents all of the aforementioned six kinetic models, respectively. Moreover, all of the constants and correlation coefficients for the kinetic models were calculated in Table 3. The data exhibited that the adsorption processes of the malachite green dye follow the pseudo-second-order model more than pseudo-first-order because the correlation coefficients of the pseudo-second-order model are greater than that of pseudo-first-order. The inner diffusion process of the malachite green dye adsorbates inside the zeolite nanostructures adsorbent particles was checked using intra-particle-diffusion model [47]. The validity of this model is known to be vital in the case of obtaining zero intercept values of the plot of Q_t vs. $t^{0.5}$. However, the plot of Q_t vs. $t^{0.5}$ produces linear fittings with good correlation coefficients which did not pass through the origin, indicating that intra-particle diffusion is not the only rate-controlling mechanism. Outer diffusion process was verified by Spahn and Schlunder [47]. Good correlation coefficients values of this model were obtained indicating that there is a dominant part of this process in the adsorption. The outer diffusion process was also confirmed via the model assumed by Iqbal et al. [47] where excellent linear relationships (with good correlation coefficients)

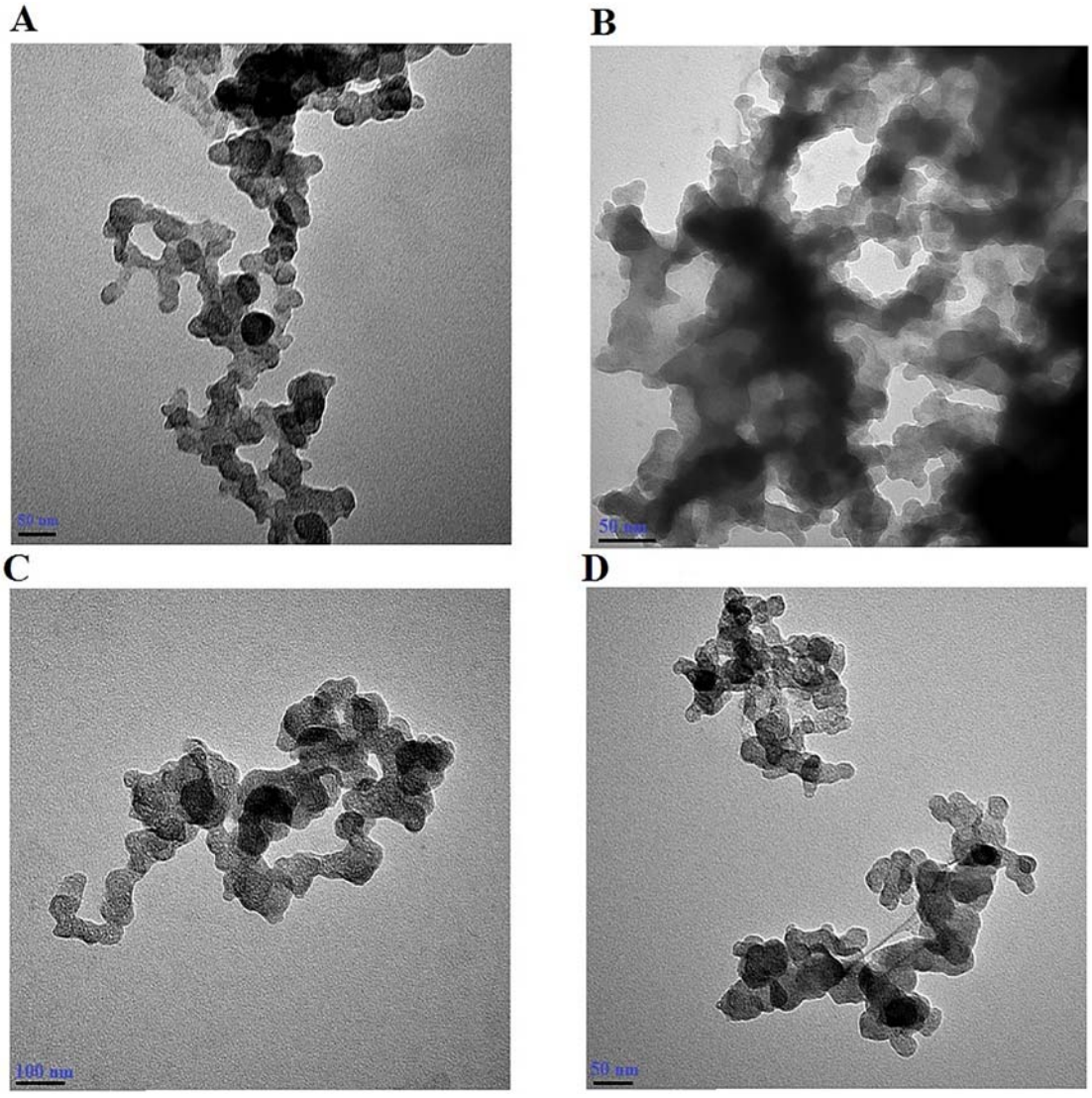

Fig. 4. TEM images of the zeolite nanostructures synthesized using fumed silica (ZF sample) (A), sodium metasilicate (ZM sample) (B), silica gel (ZS sample) (C), and tetraethyl orthosilicate (ZT sample) (D).

do not pass through the origin. Bangham model [47] prove that pore diffusion process is the only rate- controlling- step because it characterized by good correlation coefficients values. Hence, the adsorption of the malachite green dye molecules onto ZF, ZM, ZS, and ZT zeolite nanostructures takes place in three successive stages (I) Inner diffusion process (II) Outer diffusion process (III) Pore diffusion process.

3.4.2. Effect of concentration and adsorption isotherms

Fig. 8A shows that the percent removal over the as-prepared zeolite nanostructures (ZF, ZM, ZS, and ZT) increases as the concentration of the malachite green dye decreases. In addition, the experimental adsorption data were examined by fitting to two models namely, Langmuir (Eq. (16)) and Freundlich (Eq. (17)) isotherms as shown in Figs. 8B and C, respectively [47].

$C_e/Q_e = (1/bQ_m) + (C_e/Q_m)$ [16].

$$C_e/Q_e = (1/bQ_m) + (C_e/Q_m) \quad (16)$$

$$\ln Q_e = \ln K_f + (1/n) \ln C_e \quad (17)$$

where, C_e (mg/L) is the residual dye concentration at the equilibrium, Q_e (mg/g) is the amount of the adsorbed dye at the equilibrium, b (L/mg) is the Langmuir constant, Q_m (mg/g) is the maximum adsorption capacity, K_f (mg/g) (L/mg) $^{1/n}$ is the Freundlish constant and 1/n is the heterogeneity factor. Moreover, Q_m was calculated from Freundlish isotherm, using Eq. (18), as Halsey told [47].

$$Q_m = K_f(C_o)^{1/n} \quad (18)$$

All the constants for the previous two models were shown in Table 4. The results confirmed that the adsorption process fitted well with the Langmuir isotherm because their corresponding correlation coefficients more than those of Freundlish isotherm. Moreover, the maximum adsorption capacities of the malachite green dye on the as-prepared zeolite nanostructures (ZF, ZM, ZS, and ZT) adsorbents were 226.757, 239.234, 29.744, and 25.221, respectively.

3.4.3. Effect of temperature and adsorption thermodynamic parameters

Fig. 9A shows that the percent removal of the malachite green dye over the as-prepared zeolite nanostructures (ZF, ZM, ZS, and ZT) decreased largely with raising the temperature of the dye solution. Hence, the adsorption processes were exothermic. This observation may be because of the ability of the adsorbed malachite green dye molecules to escape into liquid solution again at higher temperatures. In addition, thermodynamic parameters such as a change in enthalpy (ΔH^o),

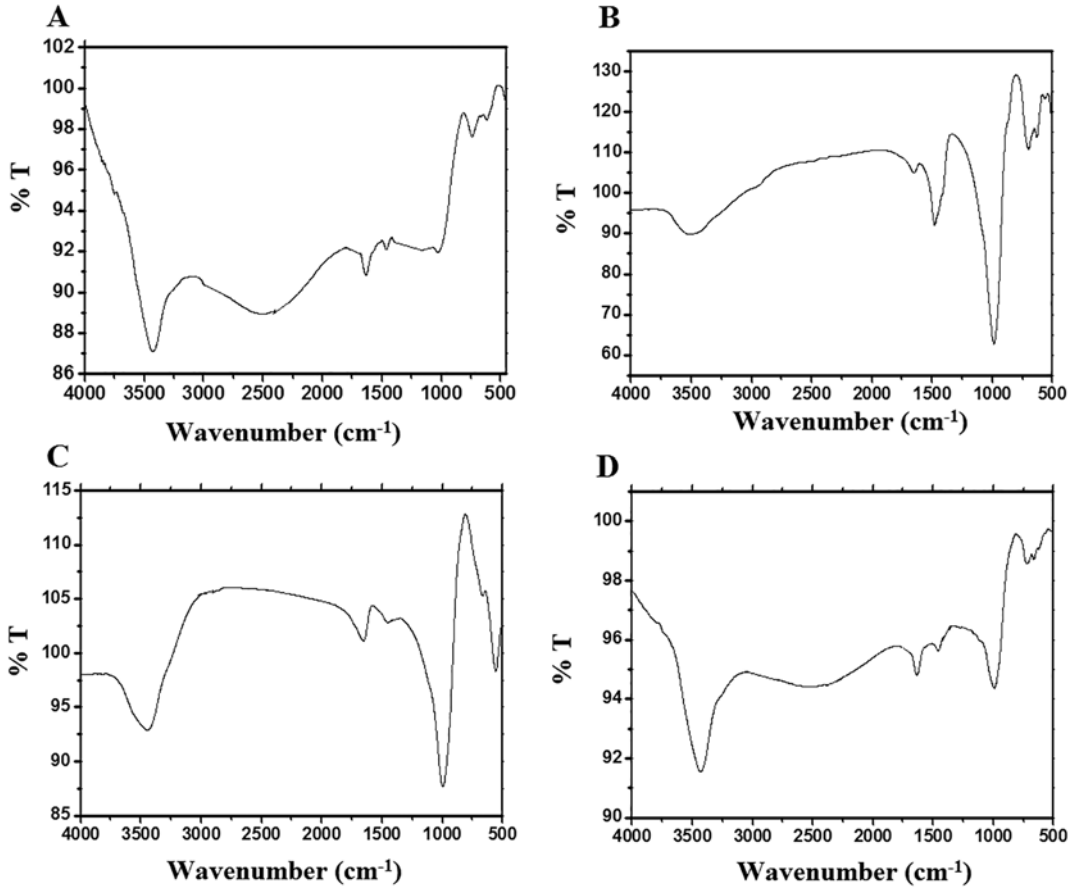

Fig. 5. FT-IR spectra of the zeolite nanostructures synthesized using fumed silica (ZF sample) (A), sodium metasilicate (ZM sample) (B), silica gel (ZS sample) (C), and tetraethyl orthosilicate (ZT sample) (D).

change in the entropy (ΔS^o), and change in free energy (ΔG^o) were calculated using Eqs. (19) and (20) [47].

$$\ln K_d = (\Delta S^o/R) - (\Delta H^o/RT) \quad (19)$$

$$\Delta G^o = \Delta H^o - T\Delta S^o \quad (20)$$

where, K_d (l/g) is distribution coefficient which is determined from either Eq. (21) or Eq. (22), T (K) is temperature, and R (KJ/mol K) is gas constant.

$$K_d = Q_T/C_T \quad (21)$$

$$K_d = [\%\text{Removal}/(100 - \%\text{Removal})]V/m \quad (22)$$

Fig. 9B and Table 5 confirms that the adsorption processes of the malachite green dye on the as-prepared zeolite nanostructures adsorbents (ZF, ZM, ZS, and ZT) are spontaneous at lower temperatures due to the obtained negative ΔG^0 values. In addition, Adsorption processes were exothermic because of the obtained negative ΔH^0 values. Due to

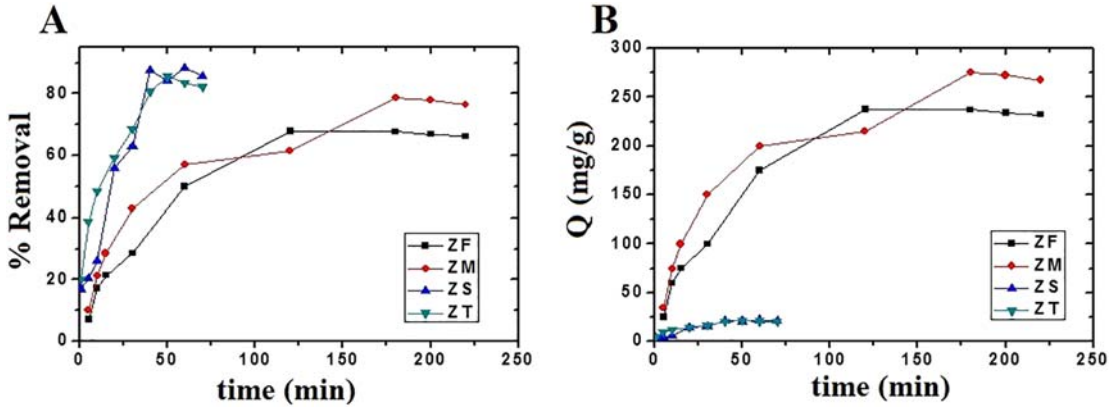

Fig. 6. Effect of contact time on both of the percent removal of malachite green dye (A) and amount of adsorbed malachite green dye (B) using ZF, ZM, ZS, and ZT samples.

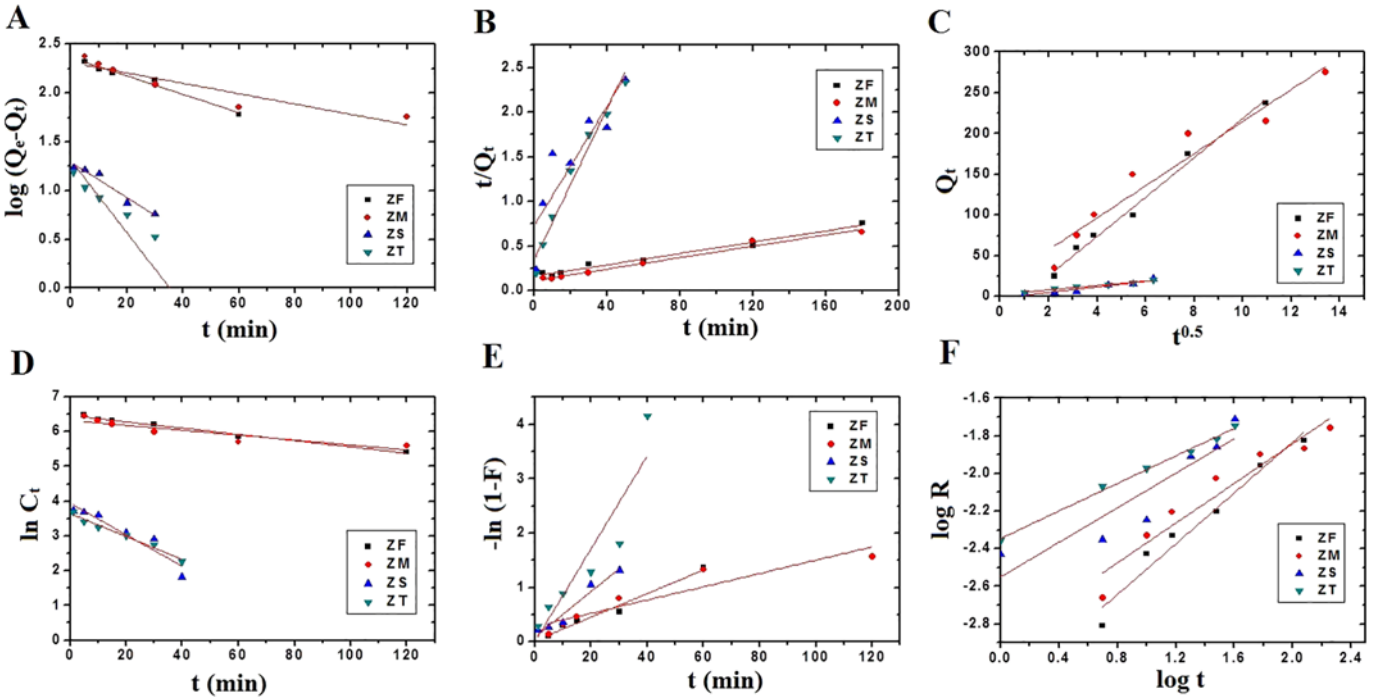

Fig. 7. Pseudo- first-order (A), Pseudo- second-order (B), Intra- particle-diffusion (C), Spahn and Schlunder (D), Iqbal et al… (E), and Bangham (F) kinetic models using ZF, ZM, ZS, and ZT samples.

the significant increase in the values of ΔG^0 at high temperatures, the processes are non-spontaneous at these temperatures. Moreover, the adsorption processes of malachite green dye on the as-prepared zeolite nanostructures (ZF, ZM, ZS, and ZT) adsorbents are physisorption because the ΔH^0 values are -5.819, -5.715, -22.620, and -22.473 kJ/mol, respectively [47]. Eventually, ZF, ZM, ZS, and ZT zeolite nanostructures were expected to be promising adsorbents and have the potential to be used as low-cost adsorbents for water purification.

4. Conclusions

Different zeolite nanostructures were synthesized via a hydrothermal method using waste aluminum cans as an aluminum source and four silicon sources namely, fumed silica, sodium metasilicate, silica gel, and tetraethyl orthosilicate. The results showed that the change of the silicon source results in an effect on the produced phase, crystallite size, and morphology. The as-prepared zeolite nanostructures possess high adsorption capacity for the removal of the malachite green dye from aqueous media. Moreover, the maximum adsorption capacities of the malachite green dye on the as-prepared zeolite nanostructures (ZF, ZM, ZS, and ZT) adsorbents were 226.757, 239.234, 29.744, and 25.221, respectively. The data exhibited that the adsorption processes of the malachite green dye follow the pseudo-second-order kinetic model and Langmuir isotherm. Besides, the results indicating that there are dominant parts of inner diffusion, outer diffusion, and pore diffusion processes in the adsorption. Bangham model proves that pore diffusion process is the only rate- controlling-step. Also, the results prove that the adsorption

Table 3
Kinetic models of the adsorption of malachite green dye on the synthesized ZF, ZM, ZS, and ZT samples.

Kinetic model	ZF			ZM			ZS			ZT		
Pseudo first order	Q_e (mg/g)	K_1 (1/min)	R^2	Q_e (mg/g)	K_1 (1/min)	R^2	Q_e (mg/g)	K_1 (1/min)	R^2	Q_e (mg/g)	K_1 (1/min)	R^2
	230.107	0.022	0.971	205.116	0.012	0.844	19.617	0.042	0.893	20.440	0.085	0.824
Pseudo second order	Q_e (mg/g)	K_2 (g/mg.min)	R^2	Q_e (mg/g)	K_2 (g/mg.min)	R^2	Q_e (mg/g)	K_2 (g/mg.min)	R^2	Q_e (mg/g)	K_2 (g/mg.min)	R^2
	314.465	6.2E−5	0.977	312.500	9.1E−5	0.976	28.629	1.7E−3	0.938	23.148	5.8E−3	0.987
Intra particle diffusion	C (mg/g)	K_{int} (mg/(g.$min^{0.5}$))	R^2	C (mg/g)	K_{int} (mg/(g.$min^{0.5}$))	R^2	C (mg/g)	K_{int} (mg/(g.$min^{0.5}$))	R^2	C (mg/g)	K_{int} (mg/(g.$min^{0.5}$))	R^2
	22.400	24.14	0.987	18.38	19.66	0.927	1.478	3.369	0.903	3.078	2.671	0.986
Spahn and Schlunder	C_o (mg/g)	K_{ext} (1/min)	R^2	C_o (mg/g)	K_{ext} (1/min)	R^2	C_o (mg/g)	K_{ext} (1/min)	R^2	C_o (mg/g)	K_{ext} (1/min)	R^2
	643.550	0.009	0.985	559.476	0.007	0.793	51.703	0.045	0.881	38.550	0.033	0.986
Iqbal et al	K_{ext} (1/min)	R^2		K_{ext} (1/min)	R^2		K_{ext} (1/min)	R^2		K_{ext} (1/min)	R^2	
	0.022	0.971		0.012	0.844		0.042	0.939		0.085	0.824	
Bangham	α (mg/g·min)	K_o (g/mg·min)	R^2	α (mg/g·min)	K_o (g/mg·min)	R^2	α (mg/g·min)	K_o (g/mg·min)	R^2	α (mg/g·min)	K_o (g/mg·min)	R^2
	0.675	7.6E−4	0.955	0.527	1.5E−3	0.911	0.406	3.5E−3	0.759	0.367	5.2E−3	0.996

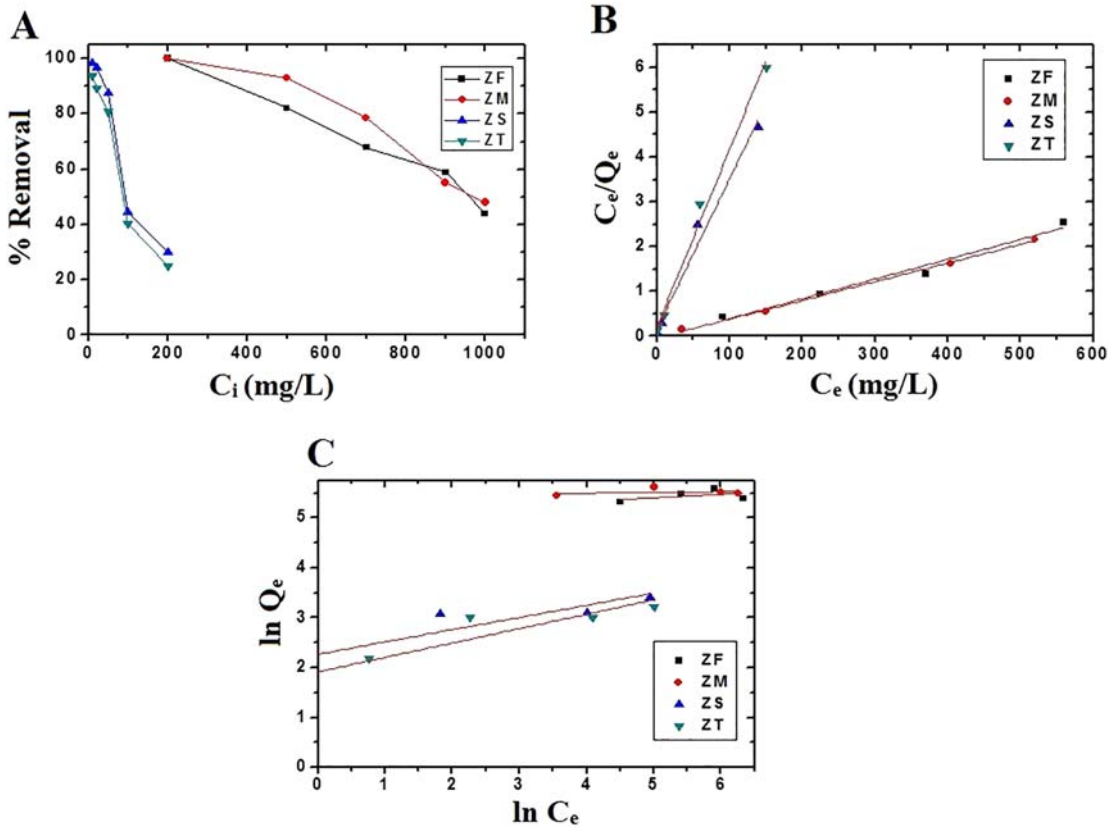

Fig. 8. Effect of initial concentrations on the removal of malachite green dye using ZF, ZM, ZS, and ZT samples (A), Langmuir isotherms (B), and Freundlish isotherms (C).

Table 4
Adsorption isotherms of the adsorption of malachite green dye on the synthesized ZF, ZM, ZS, and ZT samples.

Adsorption model	ZF			ZM			ZS			ZT		
Langmuir	Q_m (mg/g)	b (L/mg)	R^2	Q_m (mg/g)	b (L/mg)	R^2	Q_m (mg/g)	b (L/mg)	R^2	Q_m (mg/g)	b (L/mg)	R^2
	226.757	0.112	0.964	239.234	0.116	0.997	29.744	0.230	0.976	25.221	0.197	0.989
Freundlish	Q_m (mg/g)	K_f (mg/g)(L/mg)$^{1/n}$	R^2	Q_m (mg/g)	K_f (mg/g)(L/mg)$^{1/n}$	R^2	Q_m (mg/g)	K_f (mg/g)(L/mg)$^{1/n}$	R^2	Q_m (mg/g)	K_f (mg/g)(L/mg)$^{1/n}$	R^2
	244.955	154.969	−0.102	252.805	233.857	−0.443	28.099	9.725	0.862	23.801	6.838	0.818

processes are spontaneous and exothermic due to the obtained negative ΔG^0 and ΔH^0 values, respectively. Moreover, the adsorption processes are physisorption because the ΔH^0 values are less than 40 kJ/mol.

Acknowledgements

The author sincerely thanks his wife “Asmaa Elsayed Fetoh” for her continued encouragement.

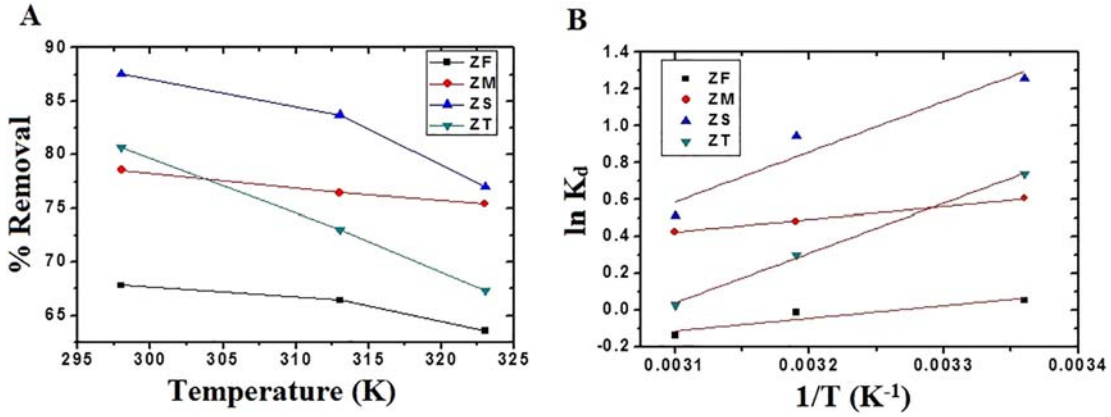

Fig. 9. Plot of % Removal of malachite green dye vs. temperature using ZF, ZM, ZS, and ZT samples (A) and plot of $\ln K_d$ vs. 1/T (B).

Table 5
Thermodynamic parameters of the adsorption of malachite green dye on the synthesized ZF, ZM, ZS, and ZT samples.

Thermodynamic parameters	ΔG° (KJ/mol)			ΔS° (KJ/mol·K)	ΔH° (KJ/mol)
	298 (K)	313 (K)	323 (K)		
ZF	−11.481	−11.766	−11.956	0.019	−5.819
ZM	−9.887	−10.097	−10.237	0.014	−5.715
ZS	−41.990	−42.965	−43.615	0.065	−22.620
ZT	−43.035	−44.070	−44.760	0.069	−22.473

References

[1] P.I. Plaza, S.A. Lambertucci, How are garbage dumps impacting vertebrate demography, heath, and conservation? Glob. Ecol. Conserv. 12 (2017) 9–20.
[2] C. Rodriguez, A. Alaswad, Z. El-Hassan, A.G. Olabi, Mechanical pretreatment of waste paper for biogas production, Waste Manag. 68 (2017) 157–164.
[3] H. Nishimura, L. Tan, N. Kira, S. Tomiyama, K. Yamada, Z.Y. Sun, Y.Q. Tang, S. Morimura, K. Kida, Production of ethanol from a mixture of waste paper and kitchen waste via a process of successive liquefaction, presaccharification, and simultaneous saccharification and fermentation, Waste Manag. 67 (2017) 86–94.
[4] R.M. Novais, J. Carvalheiras, M.P. Seabra, R.C. Pullar, J.A. Labrincha, Effective mechanical reinforcement of inorganic polymers using glass fibre waste, J. Clean. Prod. 166 (2017) 343–349.
[5] A.R.G. de Azevedo, J. Alexandre, E.B. Zanelato, M.T. Marvila, Influence of incorporation of glass waste on the rheological properties of adhesive mortar, Constr. Build. Mater. 148 (2017) 359–368.
[6] H. Lee, A. Hanif, J. Sim, H. Oh, Performance evaluation of concrete incorporating glass powder and glass sludge wastes as supplementary cementing material, J. Clean. Prod. 170 (2017) 683–693.
[7] A. Mohajerani, J. Vajna, T.H.H. Cheung, H. Kurmus, A. Arulrajah, S. Horpibulsuk, Practical recycling applications of crushed waste glass in construction materials: A review, Constr. Build. Mater. 156 (2017) 443–467.
[8] K. Ragaert, L. Delva, K. Van Geem, Mechanical and chemical recycling of solid plastic waste, Waste Manag. 69 (2017) 24–58.
[9] J. Saleem, M. Adil, G. Mckay, Oil sorbents from plastic wastes and polymers: A review, J. Hazard. Mater. 341 (2018) 424–437.
[10] C. Neffa Gobbi, V.M. Lourenço Sanches, E.B. Acordi Vasques Pacheco, M.J. de Oliveira Cavalcanti Guimarães, M.A. Vasconcelos de Freitas, Management of plastic wastes at Brazilian ports and diagnosis of their generation, Mar. Pollut. Bull. 124 (2017) 67–73.
[11] S.I. Hawash, J.Y. Farah, G. El-Diwani, Pyrolysis of agriculture wastes for bio-oil and char production, J. Anal. Appl. Pyrolysis 124 (2017) 369–372.
[12] F. Yu, L. Sun, Y. Zhou, B. Gao, W. Gao, C. Bao, C. Feng, Y. Li, Biosorbents based on agricultural wastes for ionic liquid removal: An approach to agricultural wastes management, Chemosphere 165 (2016) 94–99.
[13] O. Huerta-Pujol, M. Soliva, F. Giró, M. López, Heavy metal content in rubbish bags used for separate collection of biowaste, Waste Manag. 30 (2010) 1450–1456.
[14] R. Cayumil, R. Khanna, M. Ikram-Ul-Haq, R. Rajarao, A. Hill, V. Sahajwalla, Generation of copper rich metallic phases from waste printed circuit boards, Waste Manag. 34 (2014) 1783–1792.
[15] K.K. Rane, P.P. Date, Reduction and densification characteristics of iron oxide metallic waste during solid state recycling, Adv. Powder Technol. 26 (2015) 126–138.
[16] N. Das, G. Abraham, P. Sengupta, A. Arya, V. Kain, G.K. Dey, Microstructural analysis and corrosion behavior of zirconium-stainless steel metallic waste form, J. Nucl. Mater. 467 (2015) 489–499.
[17] V. Chapman, B.J. Welch, M. Skyllas-Kazacos, High temperature oxidation behaviour of Ni-Fe-Co anodes for aluminium electrolysis, Corros. Sci. 53 (2011) 2815–2825.
[18] A. Jing Lü, Y. Qi Shen, X. Zhong Gong, Z. Wang, Y. Hua Wang, M. Yong Wang, Effects of electrolyte recycling on desulfurization from bauxite water slurry electrolysis, Trans. Nonferrous Metals Soc. China 26 (2016) 1714–1720 (English Ed).
[19] T. Chandra Shil, Preparation of aluminum oxide from industrial waste can available in Bangladesh environment: SEM and EDX analysis, J. Adv. Chem. Eng. 6 (2016) 1–5.
[20] S. Chotisuwan, A. Sirirak, P. Har-Wae, J. Wittayakun, Mesoporous alumina prepared from waste aluminum cans and used as catalytic support for toluene oxidation, Mater. Lett. 70 (2012) 125–127.
[21] R. Galindo, A. López-Delgado, I. Padilla, M. Yates, Synthesis and characterisation of hydrotalcites produced by an aluminium hazardous waste: A comparison between the use of ammonia and the use of triethanolamine, Appl. Clay Sci. 115 (2015) 115–123.
[22] C.G. Flores, H. Schneider, N.R. Marcilio, L. Ferret, J.C.P. Oliveira, Potassic zeolites from Brazilian coal ash for use as a fertilizer in agriculture, Waste Manag. 70 (2017) 263–271.
[23] T. Abdullahi, Z. Harun, M.H.D. Othman, A review on sustainable synthesis of zeolite from kaolinite resources via hydrothermal process, Adv. Powder Technol. 28 (2017) 1827–1840.
[24] A.Á.B. Maia, R.F. Neves, Rô.S. Angélica, H. Pöllmann, Synthesis, optimisation and characterisation of the zeolite NaA using kaolin waste from the Amazon Region. Production of Zeolites KA, MgA and CaA, Appl. Clay Sci. 108 (2015) 55–60.
[25] M.A. Saada, M. Soulard, J. Patarin, R.C. Regis, Synthesis of zeolite materials from asbestos wastes: An economical approach, Microporous Mesoporous Mater. 122 (2009) 275–282.
[26] N.F. Gao, S. Kume, K. Watari, Zeolite-carbon composites prepared from industrial wastes: (I) Effects of processing parameters, Mater. Sci. Eng. A 399 (2005) 216–221.
[27] Y. Pukcothanung, T. Siritanon, K. Rangsriwatananon, The efficiency of zeolite Y and surfactant-modified zeolite Y for removal of 2,4-dichlorophenoxyacetic acid and 1,1′-dimethyl-4,4′-bipyridinium ion, Microporous Mesoporous Mater. 258 (2018) 131–140.
[28] I. Graça, M.C. Bacariza, D. Chadwick, Glucose isomerisation into fructose over Mg-impregnated Na-zeolites: Influence of zeolite structure, Microporous Mesoporous Mater. 255 (2018) 130–139.
[29] Y. Wang, D. Yang, S. Li, M. Chen, L. Guo, J. Zhou, Ru/hierarchical HZSM-5 zeolite as efficient bi-functional adsorbent/catalyst for bulky aromatic VOCs elimination, Microporous Mesoporous Mater. 258 (2018) 17–25.
[30] M. Rahmani, M. Kaykhaii, M. Sasani, Application of Taguchi L16 design method for comparative study of ability of 3A zeolite in removal of Rhodamine B and Malachite green from environmental water samples, Spectrochim. Acta A Mol. Biomol. Spectrosc. 188 (2018) 164–169.
[31] G. Kabir, A.T. Mohd Din, B.H. Hameed, Pyrolysis of oil palm mesocarp fiber catalyzed with steel slag-derived zeolite for bio-oil production, Bioresour. Technol. 249 (2018) 42–48.
[32] G. Tsintskaladze, L. Eprikashvili, N. Mumladze, V. Gabunia, T. Sharashenidze, M. Zautashvili, T. Kordzakhia, T. Shatakishvili, Nitrogenous zeolite nanomaterial and the possibility of its application in agriculture, Ann. Agric. Sci. 15 (2017) 365–369.
[33] L. Eprikashvili, M. Zautashvili, T. Kordzakhia, N. Pirtskhalava, M. Dzagania, I. Rubashvili, V. Tsitsishvili, Intensification of bioproductivity of agricultural cultures by adding natural zeolites and brown coals into soils, Ann. Agric. Sci. 14 (2016) 67–71.
[34] S. Teketel, L.F. Lundegaard, W. Skistad, S.M. Chavan, U. Olsbye, K.P. Lillerud, P. Beato, S. Svelle, Morphology-induced shape selectivity in zeolite catalysis, J. Catal. 327 (2015) 22–32.
[35] P. Losch, A.B. Pinar, M.G. Willinger, K. Soukup, S. Chavan, B. Vincent, P. Pale, B. Louis, H-ZSM-5 zeolite model crystals: Structure-diffusion-activity relationship in methanol-to-olefins catalysis, J. Catal. 345 (2017) 11–23.
[36] J. Weitkamp, Zeolites and catalysis, Solid State Ionics 131 (2000) 175–188.
[37] M. Stöcker, Gas phase catalysis by zeolites, Microporous Mesoporous Mater. 82 (2005) 257–292.
[38] H. Mola-Abasi, I. Shooshpasha, Influence of zeolite and cement additions on mechanical behavior of sandy soil, J. Rock Mech. Geotech. Eng. 8 (2016) 746–752.
[39] M. Boháč, D. Kubátová, R. Nečas, A. Zezulová, A. Masárová, R. Novotný, Properties of cement pastes with zeolite during early stage of hydration, Procedia Eng. 151 (2016) 2–9.
[40] G. Girskas, G. Skripkiūnas, The effect of synthetic zeolite on hardened cement paste microstructure and freeze-thaw durability of concrete, Constr. Build. Mater. 142 (2017) 117–127.
[41] G.V. Brião, S.L. Jahn, E.L. Foletto, G.L. Dotto, Adsorption of crystal violet dye onto a mesoporous ZSM-5 zeolite synthetized using chitin as template, J. Colloid Interface Sci. 508 (2017) 313–322.
[42] I. Humelnicu, A. Băiceanu, M.E. Ignat, V. Dulman, The removal of basic blue 41 textile dye from aqueous solution by adsorption onto natural zeolitic tuff: kinetics and thermodynamics, Process. Saf. Environ. Prot. 105 (2017) 274–287.
[43] E. Alver, A.Ü. Metin, Anionic dye removal from aqueous solutions using modified zeolite: Adsorption kinetics and isotherm studies, Chem. Eng. J. 200–202 (2012) 59–67.
[44] H. Aysan, S. Edebali, C. Ozdemir, M. Celik Karakaya, N. Karakaya, Use of chabazite, a naturally abundant zeolite, for the investigation of the adsorption kinetics and mechanism of methylene blue dye, Microporous Mesoporous Mater. 235 (2016) 78–86.
[45] N. Mirzaei, M. Hadi, M. Gholami, R.F. Fard, M.S. Aminabad, Sorption of acid dye by surfactant modificated natural zeolites, J. Taiwan Inst. Chem. Eng. 59 (2016) 186–194.
[46] M.Y. Nassar, E.A. Abdelrahman, Hydrothermal tuning of the morphology and crystallite size of zeolite nanostructures for simultaneous adsorption and photocatalytic degradation of methylene blue dye, J. Mol. Liq. 242 (2017).
[47] M.Y. Nassar, E.A. Abdelrahman, A.A. Aly, T.Y. Mohamed, A facile synthesis of mordenite zeolite nanostructures for efficient bleaching of crude soybean oil and removal of methylene blue dye from aqueous media, J. Mol. Liq. 248 (2017) 302–313.
[48] Y. Mu, Y. Zhang, J. Fan, C. Guo, Effect of ultrasound pretreatment on the hydrothermal synthesis of SSZ-13 zeolite, Ultrason. Sonochem. 38 (2017) 430–436.
[49] M. Anbia, E. Koohsaryan, A. Borhani, Novel hydrothermal synthesis of hierarchically-structured zeolite LTA microspheres, Mater. Chem. Phys. 193 (2017) 380–390.
[50] L.V. Sousa, A.O.S. Silva, B.J.B. Silva, C.M. Teixeira, A.P. Arcanjo, R. Frety, J.G.A. Pacheco, Fast synthesis of ZSM-22 zeolite by the seed-assisted method of crystallization with methanol, Microporous Mesoporous Mater. 254 (2017) 192–200.

[51] L.B. Bortolatto, R.A.A. Boca Santa, J.C. Moreira, D.B. Machado, M.A.P.M. Martins, M.A. Fiori, N.C. Kuhnen, H.G. Riella, Synthesis and characterization of Y zeolites from alternative silicon and aluminium sources, Microporous Mesoporous Mater. 248 (2017) 214–221.
[52] R. Sabarish, G. Unnikrishnan, Synthesis, characterization and catalytic activity of hierarchical ZSM-5 templated by carboxymethyl cellulose, Powder Technol. 320 (2017) 412–419.
[53] Y.H. Hsiao, T.Y. Ho, Y.H. Shen, D. Ray, Synthesis of analcime from sericite and pyrophyllite by microwave-assisted hydrothermal processes, Appl. Clay Sci. 143 (2017) 378–386.
[54] X. Ma, J. Yang, H. Ma, C. Liu, P. Zhang, Synthesis and characterization of analcime using quartz syenite powder by alkali-hydrothermal treatment, Microporous Mesoporous Mater. 201 (2015) 134–140.
[55] M. Esaifan, M. Hourani, H. Khoury, H. Rahier, J. Wastiels, Synthesis of hydroxysodalite zeolite by alkali-activation of basalt powder rich in calc-plagioclase, Adv. Powder Technol. 28 (2017) 473–480.
[56] B. Muir, J. Matusik, T. Bajda, New insights into alkylammonium-functionalized clinoptilolite and Na-P1 zeolite: Structural and textural features, Appl. Surf. Sci. 361 (2016) 242–250.
[57] M. Barkat, D. Nibou, S. Amokrane, S. Chegrouche, A. Mellah, Uranium (VI) adsorption on synthesized 4A and P1 zeolites: Equilibrium, kinetic, and thermodynamic studies, C. R. Chim. 18 (2015) 261–269.
[58] A.M. Cardoso, M.B. Horn, L.S. Ferret, C.M.N. Azevedo, M. Pires, Integrated synthesis of zeolites 4A and Na-P1 using coal fly ash for application in the formulation of detergents and swine wastewater treatment, J. Hazard. Mater. 287 (2015) 69–77.
[59] H. Wang, Q. Feng, K. Liu, Z. Li, X. Tang, G. Li, Highly efficient fluoride adsorption from aqueous solution by nepheline prepared from kaolinite through alkali-hydrothermal process, J. Environ. Manag. 196 (2017) 72–79.
[60] E.Z. Hegazy, I.H.A. El Maksod, R.M.M.A. El Enin, Preparation and characterization of Ti and V modified analcime from local kaolin, Appl. Clay Sci. 49 (2010) 149–155.
[61] J.E. Oh, J. Moon, M. Mancio, S.M. Clark, P.J.M. Monteiro, Bulk modulus of basic sodalite, $Na_8[AlSiO_4]_6(OH)_2 \cdot 2H_2O$, a possible zeolitic precursor in coal-fly-ash-based geopolymers, Cem. Concr. Res. 41 (2011) 107–112.
[62] J. Xie, W. Meng, D. Wu, Z. Zhang, H. Kong, Removal of organic pollutants by surfactant modified zeolite: Comparison between ionizable phenolic compounds and non-ionizable organic compounds, J. Hazard. Mater. 231–232 (2012) 57–63.
[63] B.I. Hassan, H.D. Grundy, Structure of basic sodalite $Na_8Al_8Si_6O_{24}(OH)_2 \cdot 2H_2O$, Acta Crystallogr. 39 (1983) 3–5.
[64] M.M.J. Treacy, J.B. Higgins, Collection of simulated XRD powder patterns for, Zeolites 1 (2001) 192–193.
[65] S. Hansen, L. Falth, X-ray study of the nepheline hydrate I structure, Zeolites 2 (1982) 162–166.
[66] M. Jafari, A. Nouri, M. Kazemimoghadam, T. Mohammadi, Investigations on hydrothermal synthesis parameters in preparation of nanoparticles of LTA zeolite with the aid of TMAOH, Powder Technol. 237 (2013) 442–449.
[67] X. Ni, Z. Zheng, X. Wang, S. Zhang, M. Zhao, Fabrication of hierarchical zeolite 4A microspheres with improved adsorption capacity to bromofluoropropene and their fire suppression performance, J. Alloys Compd. 592 (2014) 135–139.
[68] M.Y. Nassar, H.M. Aly, E.A. Abdelrahman, M.E. Moustafa, Synthesis, characterization, and biological activity of some novel Schiff bases and their Co(II) and Ni(II) complexes: A new route for Co_3O_4 and NiO nanoparticles for photocatalytic degradation of methylene blue dye, J. Mol. Struct. 1143 (2017) 462–471.
[69] H.M. Aly, M.E. Moustafa, M.Y. Nassar, E.A. Abdelrahman, Synthesis and characterization of novel Cu (II) complexes with 3-substituted-4-amino-5-mercapto-1,2,4-triazole Schiff bases: A new route to CuO nanoparticles, J. Mol. Struct. 1086 (2015) 223–231.
[70] Z.M. El-bahy, M.M. Mohamed, F.I. Zidan, M.S. Thabet, Photo-degradation of acid green dye over Co – ZSM-5 catalysts prepared by incipient wetness impregnation technique, J. Hazard. Mater. 153 (2008) 364–371.
[71] C. Liu, D. Kong, H. Guo, Microporous and mesoporous materials the morphology control of zeolite ZSM-5 by regulating the polymerization degree of silicon and aluminum sources, Microporous Mesoporous Mater. 193 (2014) 61–68.